Journal of Alloys and Compounds 523 (2012) 83–87

Contents lists available at SciVerse ScienceDirect

Journal of Alloys and Compounds

journal homepage: www.elsevier.com/locate/jallcom

Effect of Mn doping on the structural and optical properties of SnO_2 nanoparticles

Ameer Azam[a,b,*], Arham S. Ahmed[b], Sami S. Habib[a], A.H. Naqvi[b]

[a] Centre of Nanotechnology, King Abdulaziz University, Jeddah, Saudi Arabia
[b] Centre of Excellence in Materials Science (Nanomaterials), Department of Applied Physics, Aligarh Muslim University, Aligarh, India

ARTICLE INFO

Article history:
Received 3 October 2011
Received in revised form 8 January 2012
Accepted 15 January 2012
Available online 28 January 2012

Keywords:
Sol–gel process
X-ray diffraction
TEM
Luminescence

ABSTRACT

Mn doped SnO_2 nanoparticles were synthesized by sol–gel method and characterized by X-ray diffraction (XRD), transmission electron microscopy (TEM), energy dispersive X-ray analysis (EDAX), UV-Visible absorption spectroscopy, photoluminescence (PL), Fourier transform infrared spectroscopy (FTIR) and Raman spectroscopy measurements. XRD analysis revealed the formation of single phase rutile type tetragonal structure of all samples which was further supported by Raman studies and FTIR measurements. Crystallite size was observed to vary from 16.2 nm to 7.1 nm as the Mn content increased from 0% to 15%, suggesting the prevention of crystal growth with Mn doping. It was evident from the absorption spectra that the absorbance tends to increase with the increase in dopant concentration. Optical band gap was calculated using Tauc relation and found to increase with the increase in Mn content confirming the size reduction as a result of Mn doping. Raman spectroscopy measurement depicted the broadening of most intense Raman peak observed at 630 cm^{-1} with Mn doping, indicating that the Mn ions are substituted at the Sn sites in SnO_2 matrix. Room temperature PL spectra revealed that the intensity of luminescent emission tends to increase with the increase in Mn concentration.

1. Introduction

Synthesis and characterization of nanoscale materials is gaining popularity among the scientific community for fundamental as well as applied research point of view because many material properties change drastically as particle size reaches the nanometer range. The optical properties of nanocrystalline semiconductors have been studied extensively in recent years for translating their enhanced properties into practical applications. As the size of the material becomes smaller, the band gap becomes larger thereby changing the optical and electrical properties of the material and making the material suitable for new applications and devices. Tin oxide (SnO_2) is one of the most important n-type wide-band gap (3.6 eV) semiconductor. Its unique conductance has been utilized for various applications like gas sensors [1], microelectronics [2], solar cells [3] and photoelectrochemistry [4]. The compound has also been examined as possible electrode material for lithium cells [5] and photocatalysts [6]. As an n-type semiconductor, SnO_2 shows very high sensitivity towards reducing gases such as H_2, CO, hydrocarbon, and alcohol. It combines the low electrical resistance with high transparency in visible range and high reflectivity in infra-red region. This property of SnO_2 makes it a prominent candidate for optoelectronic applications. The optoelectronic properties such as photoluminescence and optical band gap of SnO_2 can also be improved by impurity doping. Many results have shown that several dopants (Co, Fe, Cu) can lead to an increase of surface area of SnO_2 by reducing the grain size and crystallanity [7–9]. Several authors have studied the effect of transition metal ions (Fe, Co, Ni, Cu) on the optical and electrical properties of SnO_2 nanoparticles [7–11]. Azam et al. studied the electrical properties of Ni-doped SnO_2 nanoparticles and reported that the ac conductivity increases with Ni content [10]. Ahmed et al. discussed fluorescence properties of Ni-doped SnO_2 nanoparticles and reported that the visible emission increases as the dopant concentration increases [11]. Fang et al. reported the luminescence properties of Co-doped SnO_2 nanoparticles; they have shown that the blue emission increases with the increase in Co-doping [12].

Various approaches have been adopted for the synthesis of SnO_2 nanoparticles including the hydrothermal method [13,14], solvothermal method [15], gel-combustion method [16] and sol–gel method [17]. Amongst all, the sol–gel method for the synthesis of SnO_2 nanoparticles has a number of advantages including low temperature processing and molecular level homogeneity.

This paper reports the effect of Mn doping on the structural and optical properties of SnO_2 nanoparticles prepared by sol–gel

* Corresponding author at: Centre of Nanotechnology, King Abdulaziz University, Jeddah, Saudi Arabia. Tel.: +966 531185621; fax: +966 26951566.
E-mail addresses: azam222@rediffmail.com, ameerazam2009@gmail.com (A. Azam).

0925-8388/$ – see front matter © 2012 Elsevier B.V. All rights reserved.
doi:10.1016/j.jallcom.2012.01.072

method. Analyses were carried out using techniques like XRD, TEM, EDAX, FTIR, Raman, UV-Visible and PL spectroscopy.

2. Experimental

Details of synthesis of pure and Mn doped SnO_2 nanoparticles are reported in our earlier communication [18]. Analytical grade $SnCl_4{\cdot}5H_2O$ and $MnCl_2{\cdot}4H_2O$ were used as starting materials for the synthesis of $Sn_{1-x}Mn_xO_2$ series. In a typical synthesis procedure, citric acid was added to 100 ml of distilled water with magnetic stirring, until pH becomes 1.5. Required amounts of $SnCl_4{\cdot}5H_2O$ and (x = 0, 0.03, 0.05, 0.07, 0.09 and 0.15) $MnCl_2{\cdot}4H_2O$ were added to the solution and dissolved completely. 10 ml of ethylene glycol was added to the above solution and stirred for 20 min. Sufficient amount of aqueous ammonia (15 mol/L) was added drop wise under magnetic stirring. The resulting solution was stirred for 30 min. Finally, a gel was obtained which was washed several times with water and ethanol. Gel was dried at 120 °C for 15 h in an oven. The dried powder was further calcined at 400 °C for 2 h resulting in the formation of Mn-doped SnO_2 nanoparticles. Crystallanity, structure and crystallite size of Mn-doped SnO_2 nanoparticles were determined by XRD (Rigaku) using Cu-Kα radiations (λ = 0.15406 nm) in 2θ range from 20° to 80°. Morphological analysis was carried out using an HRTEM (JEM2100, JEOL). The compositional analysis was carried out using EDAX analysis (Oxford Instruments). Fourier transform infrared (FT-IR) spectra of the powders (as pellets in KBr) were recorded using a Fourier transform infrared spectrometer (Spectrum 65, Perkin Elmer) in the range of 4000–400 cm^{-1} with a resolution of 1 cm^{-1}. In order to get the phonon vibrational study of the pure and Mn doped SnO_2, a micro-Raman spectrometer (NRS-3100, JASCO) with a 532 nm solid state primary laser as an excitation source at room temperature was used. The room temperature PL measurements at excitation wavelength 325 nm were carried out using a luminescence spectrometer ((LS-55B, Perkin–Elmer).

3. Results and discussion

3.1. Structural properties

3.1.1. X-ray diffraction analysis

The characteristic XRD spectra of the pure and Mn-doped SnO_2 nanoparticles annealed at 400 °C are depicted in Fig. 1. The peak positions of each sample exhibit the rutile structure of SnO_2 which were very well matched with the standard ICDD card No. 77-0452 without any characteristic peaks of impurities, confirming the single phase formation of the material. Table 1 shows the variation of crystallite size, lattice parameter and cell volume of different samples. It can be observed from Table 1 that the crystallite size of SnO_2 nanoparticles reduced from 16.2 nm to 7.1 nm as a result of increase in Mn content from 0% to 15%, indicating that the presence of Mn ions in SnO_2 prevented the growth of crystal grains. Furthermore, the lattice parameters and cell volume are observed to decrease with the increase in Mn content. This suggests that Mn ions are inclined to incorporate into the lattice in the form of Mn^{+3} (65 pm) or Mn^{+4} (54 pm), since their ionic radius is smaller than that of Sn^{+4} (71 pm) [19]. It is also clear from the data that the doping of Mn in SnO_2 not only lowers the crystallite size but also degrades the crystallanity of the material. These results agree very well with the results reported earlier in literature [19]. It is also evident from Fig. 1 that as the Mn content increases, the intensity of XRD peaks decreases and FWHM increases which shows the degradation of crystallanity. This means that Mn doping in SnO_2 produces crystal defects around the dopants and the charge imbalance arised from these defects changes the stoichiometry of the materials. Similar results have also been observed and reported in our earlier communication [18].

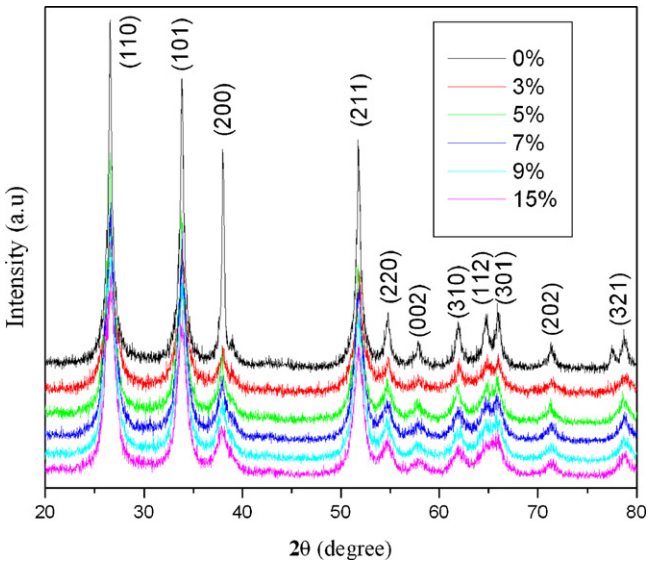

Fig. 1. XRD spectra of pure and Mn doped SnO_2 nanoparticles.

Fig. 2(a) and (b) shows TEM images taken for pure and 9% Mn-doped SnO_2 nanoparticles, respectively. It is clear from Fig. 2 that SnO_2 grains have a spherical morphology with an average diameter of 19 nm for pure SnO_2 and 8 nm for 9% Mn-doped SnO_2, confirming the reduction in particle size as a result of Mn doping in SnO_2. The particle size obtained using TEM is in well agreement with the size calculated by XRD data. Fig. 3 exhibits the corresponding selected area electron diffraction (SAED) patterns of pure (a) and Mn doped SnO_2 (b) nanoparticles. The SAED patterns show that all the polycrystalline rings are indexed to rutile structure of SnO_2 which are in good agreement with XRD results. Fig. 4 depicts EDAX spectra of pure and 9% Mn doped SnO_2 nanoparticles, which clearly shows the existence of Mn ions in doped sample and confirms the successful doping of Mn in SnO_2.

3.1.2. FT-IR analysis

FT-IR spectra were recorded in solid phase using KBr pellet technique in the region 4000–400 cm^{-1}. FT-IR spectra of all the samples are shown in the Fig. 5. It is clear from Fig. 5 that there are clear

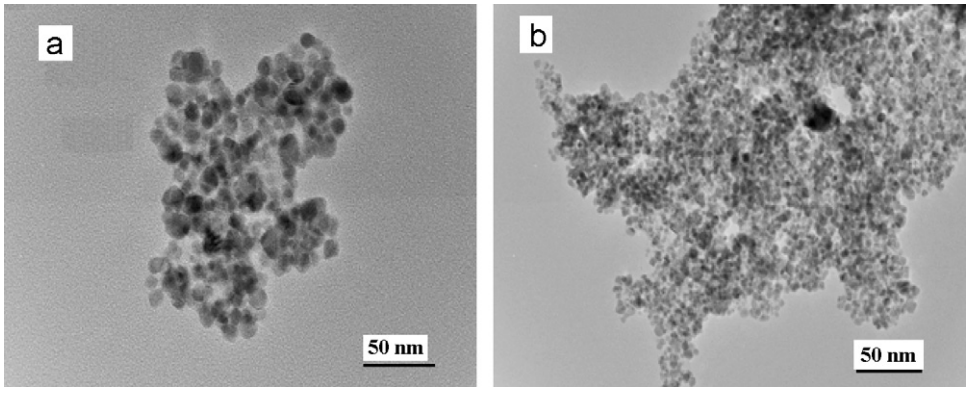

Fig. 2. TEM images of (a) pure SnO_2 and (b) 9% Mn doped SnO_2 nanoparticles.

Table 1
Variation of crystallite size, lattice parameters, cell volume and band gap with doping.

Mn concentration (%)	Crystallite size (nm)	Lattice parameters		Cell volume (Å^3)	Band gap (eV)
		a (Å)	c (Å)		
0	16.2	4.800	3.205	73.843	3.71
3	10.5	4.793	3.199	73.490	3.77
5	10.3	4.791	3.191	73.245	3.81
7	8.2	4.788	3.190	73.130	3.85
9	7.5	4.779	3.188	72.810	3.90
15	7.1	4.775	3.185	72.619	4.00

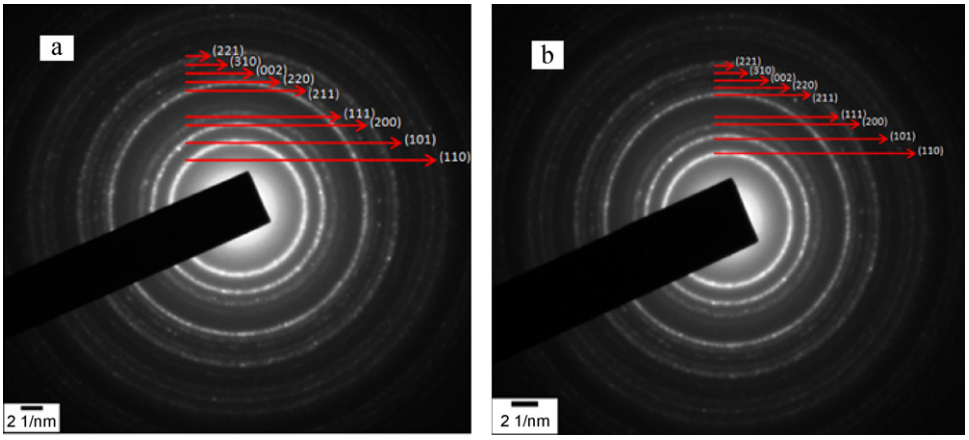

Fig. 3. SAED patterns of (a) pure SnO_2 and (b) 9% Mn doped SnO_2 nanoparticles.

changes in the positions and sizes of IR peaks indicating that Mn have been incorporated in SnO_2 host matrix. The band observed at 620 cm^{-1} may be assigned to the antisymmetric Sn—O—Sn stretching mode, while the band observed in the region 480–510 cm^{-1} can be attributed to symmetric Sn—O—Sn and Mn—O bonds. The peak appearing at 1120 cm^{-1} is related to the vibration of hydroxyl-tin (Sn—OH) bond. The vibration at 1380 cm^{-1} is assigned to the C—O stretching mode related to the citrate complex. In solid citrate the carboxylic groups are ionized, so the peak at 1625 cm^{-1} is assigned to C=O stretching vibration. The present assignments corroborate well with the values reported in available literature [20,21]. The prominent bands around 3400 and 1630 cm^{-1} account for the presence of absorbed molecular water.

3.1.3. Raman spectral study

In order to confirm the substitution of Mn^{+3} ions and to understand the effect of nanoparticles on the vibrational properties, Raman spectroscopy measurements were carried out. It is well known that SnO_2 has a tetragonal structure having two tin atoms and four oxygen atoms per unit cell with a space group D_{4h}^{14} ($P4_2/mnm$). Six unit cell atoms give a total of 18 vibrational modes in the first Brillouin Zone. The mechanical representation of all the normal modes at the center of the Brillouin zone is given by [22]

$$\Gamma = \Gamma_1^+(A_{1g}) + \Gamma_2^+(A_{2g}) + \Gamma_3^+(B_{1g}) + \Gamma_4^+(B_{2g}) + \Gamma_5^-(E_g) + 2\Gamma_1^-(A_{2u}) + 2\Gamma_4^-(B_{1u}) + 4\Gamma_5^+(E_u) \quad (2)$$

The modes A_{1g}, B_{1g}, B_{2g} and E_g are Raman active while A_{2u} and E_u are infrared active.

The room temperature Raman spectra of all the samples are shown in Fig. 6. Three fundamental Raman peaks at 485, 630, and 770 cm^{-1}, corresponding to the E_g, A_{1g}, and B_{2g} vibration modes, respectively, are observed and are in good agreement with those

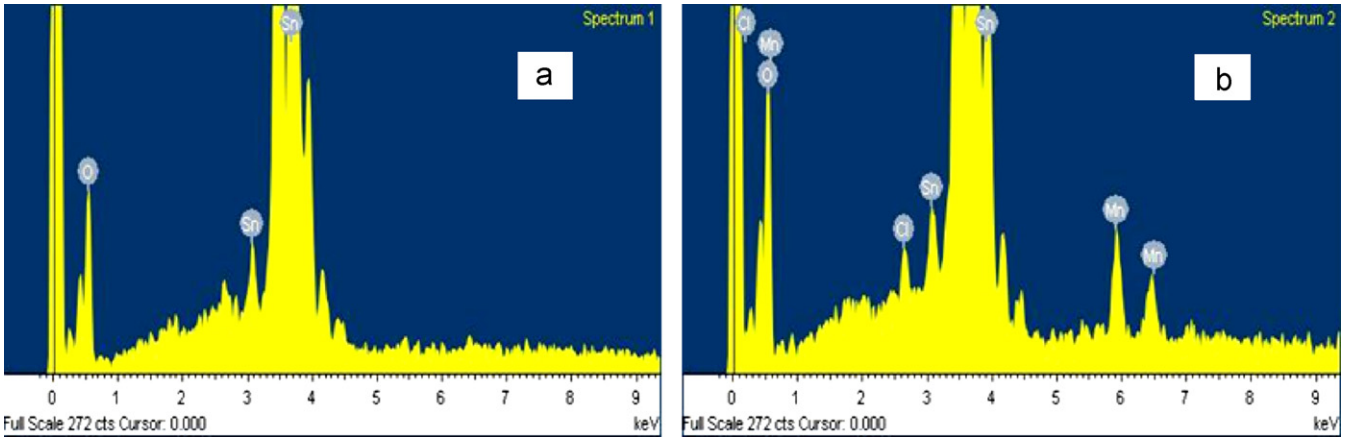

Fig. 4. EDAX spectra of (a) pure SnO_2 and (b) 9% Mn doped SnO_2 nanoparticles.

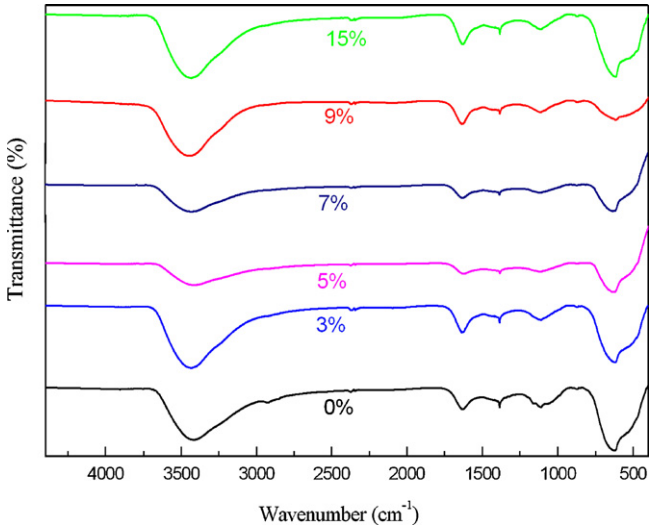

Fig. 5. FTIR spectra of all the samples.

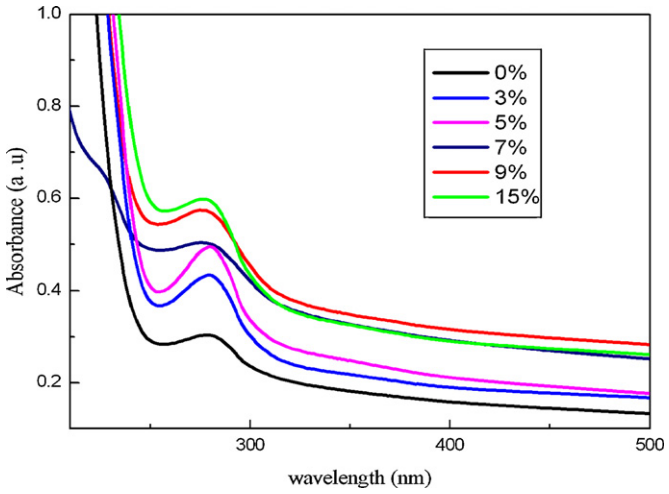

Fig. 7. Optical absorbance spectra of all the samples.

for the rutile bulk SnO_2. Thus, these peaks further confirm that the as-synthesized SnO_2 nanoparticles possess the characteristics of the tetragonal rutile structure [23]. It is interesting to note that the substitution of Mn in the SnO_2 lattice decreases the intensities of Raman peaks indicating that the Mn substitution might be responsible for the changes in local disorder and defects such as vacant lattice sites or vacancy cluster. The most intense peak observed at 630 cm^{-1} which is attributed to the A_{1g} mode, while those occurred at 485 and 770 cm^{-1} may be attributed to vibrational modes E_g and B_{2g} respectively. The modes A_{1g} (~630 cm^{-1}) and B_{2g} (~770 cm^{-1}) might be related to the expansion and contraction of vibrating mode of Sn—O bonds, while E_g mode may be related to the vibration of oxygen in oxygen plane. Apart from this, one more peak is observed at around 310 cm^{-1}. This extra peak can be attributed to the fact that in nanocrystalline system surface properties are sensitive to the grain size as well as oxygen vacancies and defects, so there may be a possibility of the appearance of new modes in Raman spectra [22]. Further, there is a continuous broadening in Raman peaks with the decrease in crystallite size which may be due to the phonon confinement effect. Similar observations have been reported in many nanomaterials such as ZnO, CeO_2, TiO_2, etc. [24–26].

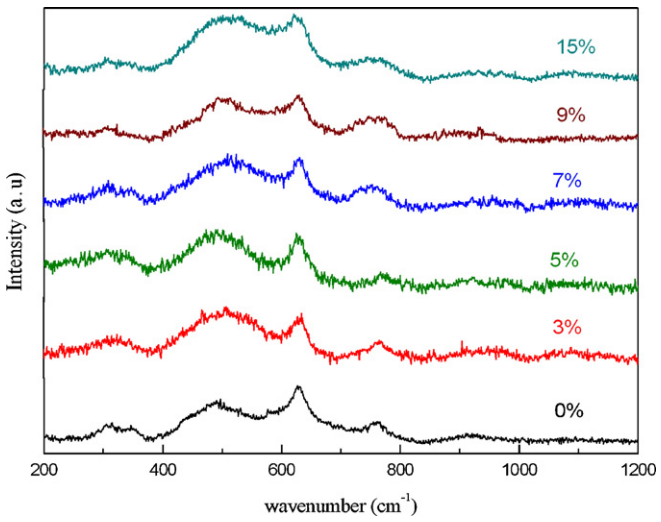

Fig. 6. Raman spectra of pure and Mn doped SnO_2 nanoparticles.

3.2. Optical properties

Absorption and fluorescence spectroscopy are powerful non-destructive techniques to explore the optical properties of semiconducting nanoparticles. In order to determine the optical band gaps and associated properties, the optical absorbance measurements were carried out at room temperature and the absorbance spectra of pure and Mn doped SnO_2 nanoparticles are shown in Fig. 7. The absorbance is expected to depend on several factors, such as band gap, oxygen deficiency surface roughness and impurity centers [11]. Absorbance spectra exhibit an absorption peak at around 280 nm which can be attributed to the photo-excitation of electrons from valence band to conduction band. The absorption edge of different samples varies as the concentration of Mn in the SnO_2 nanoparticles varies. It has been observed that the absorbance tends to increase with the increase in dopant concentration. In order to calculate the direct band gap Tauc relation was used:

$$\alpha h\nu = A(h\nu - E_g)^n$$

where α is the absorption coefficient, A is a constant. $n = 1/2$ for direct band gap semiconductor. An extrapolation of the linear region of a plot of $(\alpha h\nu)^2$ vs $h\nu$ gives the value of the optical band gap E_g. The measured band gap was found to be 3.71 eV for undoped SnO_2 nanoparticles (Table 1), which is higher than the reported value of the bulk SnO_2, i.e. 3.6 eV. This can be attributed to the quantum confinement effect of the nanoparticles [27]. On the quantum confinement of an electron–hole pair in a spherical well the band gap energy is determined by the characteristic distance (or radius, R) in the following equation [12].

$$E_g(R) + E_g^0 + \frac{h^2\pi^2}{2\mu R^2} - \frac{1.786e^2}{\varepsilon R} - \frac{0.124e^4\mu}{\hbar^2\varepsilon^2}$$

where ε is the dielectric constant and R is the particle radius and $\hbar$ is the Planck constant and $\mu = (1/m_e^* + 1/m_h^*)^{-1}$. m_e^* and m_h^* are the effective masses of electron and hole respectively. It is clear from this equation that as the particle size decreases band gap increases. The data presented in Table 1 shows that the band gap is increasing as the Mn content is increasing confirming the reduction in particle size. These observations substantiate the results obtained by XRD and TEM analysis. The change in band gap suggests that the size and shape of the nanoparticles influence the opto-electronic properties of the materials and can be tuned by doping. Similar observations have been reported for boron nitride-functionalized SnO_2

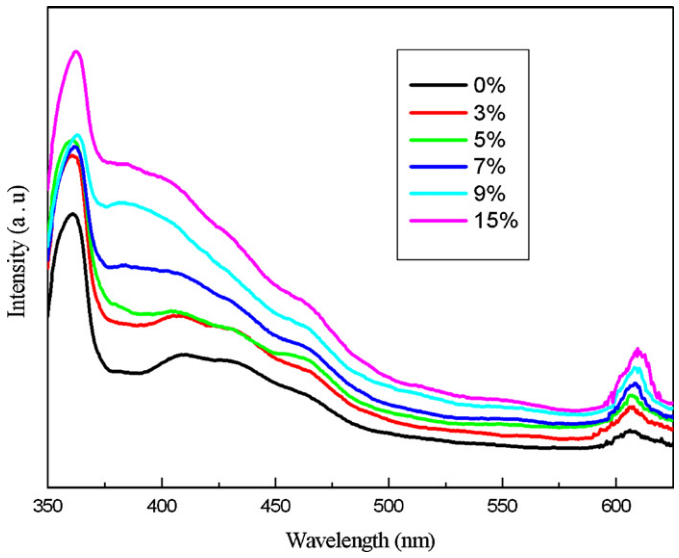

Fig. 8. Photoluminescence spectra of different samples.

nanotubes, where the band gap value was reported as 4.8 eV [28]. This is in agreement to the normal phenomenon of quantum confinement. Fang et al. have also reported the increase in band gap in Co doped SnO_2 nanoparticles [12].

The room temperature PL behaviors of pure and Mn doped SnO_2 nanoparticles were investigated using fluorescence spectrophotometer and the results are shown in Fig. 8. It can be seen from PL spectra that the samples exhibit a strong emission band at 360 nm and 612 nm, while a weak emission band located at 405 nm is also observed. It is believed that the emission wavelength of the oxide material depends mainly on the particle's shape, size, and excitation wavelength. It is well known that the visible emission of SnO_2 is related to the defect levels within the band gap, such as O vacancies and Sn interstitials formed during the particle growth [29]. The peak at 360 nm is generally ascribed to the band to acceptor transition and related to the impurity or defect concentration. The emission peak at 405 nm can be attributed to structural defects or luminescent centers, such as nanocrystals and defects in SnO_2 nanoparticles. Finally, the emission peak occurring at 612 nm is likely to originate from oxygen vacancies. Moreover, it can be seen from Fig. 8 that the intensity of luminescent emission increases with the increase in dopant concentration, which may be attributed to the increase in oxygen vacancies as a function of dopant concentration. In pure SnO_2 host, the emission attributes to electron transmission, mediated by defects levels in the band gap, such as oxygen vacancies, tin interstitials and so forth. Probably, after incorporating Mn ions into the SnO_2 host matrix, the defect still plays a dominant role with respect to the luminescence processes. Generally, oxygen vacancies are known to be the most common defects and usually act as radiative centers in luminescence processes. This may be the reason for the increment in the PL intensity after introducing the Mn ions into the SnO_2 matrix.

4. Conclusions

In summary, Mn-doped SnO_2 nanoparticles were successfully synthesized using sol–gel method. The XRD spectra exhibit the rutile type tetragonal structure of all the samples and no impurity phase was observed in XRD. It was found that with the increase in manganese concentration there was a decrease in the crystallanity, crystallite size and lattice constant. The three fundamental Raman modes of SnO_2 nanoparticles also confirm the rutile symmetry of all the samples. Optical band gap was found to vary from 3.71 eV to 4.0 eV with doping suggesting the reduction in particle size as a result of doping. The photoluminescence study showed an increase in the luminescent emission with the increase in dopant concentration. Finally, structural and optical studies conclude that the Mn ions are successfully incorporated into the lattice position of Sn in SnO_2 matrix and the process may be used to modulate the band gap and particle size and hence the material may be used in opto-electronic devices.

Acknowledgement

Mr. Arham S. Ahmed is thankful to CSIR, New Delhi for providing financial support in the form of SRF.

References

[1] R.S. Niranjan, Y.K.H. Wang, D.K. Kim, S.H. Jhung, J.S. Chang, I.S. Mulla, Mater. Chem. Phys. 92 (2005) 384.
[2] S. Schiller, U. Heisig, K. Goedicke, H. Bilz, K. Steinfelder, Thin Solid Films 92 (1982) 81.
[3] S.C. Lee, J.H. Lee, T.S. Oh, Y.H. Kim, Sol. Energy Mater. Sol. Cells 75 (2003) 481.
[4] T. Stergiopoulos, I.M. Arabatzis, H. Cachet, P. Falaras, J. Photochem. Photobiol. A Chem. 155 (2003) 163.
[5] D. Aurbach, A. Nimberger, B. Markovasky, E. Levi, E. Sominsky, A. Gedanken, Chem. Mater. 14 (2002) 4155.
[6] M. Miyauchi, A. Nikajima, T. Watanabe, K. Hasimoto, Chem. Mater. 14 (2002) 2812.
[7] H. Jin, Y. Xu, G. Pang, W. Dong, Q. Wan, Y. Sun, S. Feng, Mater. Chem. Phys. 85 (2004) 58.
[8] J. Hays, A. Punnoose, R. Baldner, M.H. Engelhard, J. Peloquin, K.M. Reddy, Phys. Rev. B 72 (2005) 075203.
[9] G. Korotcenkov, V. Macsanov, V. Brinzari, V. Tolstoy, J. Schwank, A. Cornet, J. Morante, Thin Solid Films 467 (2004) 209.
[10] A. Azam, A.S. Ahmed, M.S. Ansari, M. Muhamed Shafeeq, A.H. Naqvi, J. Alloys Compd. 506 (2010) 237.
[11] A.S. Ahmed, M. Muhamed Shafeeq, M.L. Singla, S. Tabassum, A.H. Naqvi, A. Azam, J. Lumin. 131 (2011) 1.
[12] L.M. Fang, X.T. Zu, Z.J. Li, S. Zhu, C.M. Liu, L.M. Wang, F. Gao, J. Mater. Sci.: Mater. Electron. 19 (2008) 868.
[13] H. Zhu, D. Yang, G. Yu, H. Zhang, K. Yao, Nanotechnology 17 (2006) 2386.
[14] F. Du, Z. Guo, G. Li, Mater. Lett. 59 (2005) 2563.
[15] Y. Liu, F. Yang, X. Yang, Colloids Surfaces A 312 (2008) 219.
[16] L. Fraigi, D.G. Lamas, N.E.W. Reca, Nanostruct. Mater. 11 (1999) 311.
[17] S.V. Manorama, C.V. Gopal Reddy, V.J. Rao, Nanostruct. Mater. 11 (1999) 643.
[18] A. Azam, A.S. Ahmed, M. Chaman, A.H. Naqvi, J. Appl. Phys. 108 (2010) 094329.
[19] Z.M. Tian, S.L. Yuan, J.H. He, P. Li, S.Q. Zhang, C.H. Wang, Y.Q. Wang, S.Y. Yin, L. Liu, J. Alloys Compd. 466 (2008) 26.
[20] J.-J. Zhu, J.-M. Zhu, X. Liao, J. Fang, M. Zhou, H. Chen, Mater. Lett. 53 (2002) 12.
[21] P.G. Harrison, A. Guest, J. Chem. Soc. Faraday Trans. 1 83 (1987) 3383.
[22] K. Srinivas, M. Vithal, B. Sreedhar, M.M. Raja, P.V. Reddy, J. Phys. Chem. C 113 (2009) 3543.
[23] W. Wang, C. Xu, G. Wang, Y. Liu, C. Zheng, J. Appl. Phys. 92 (2002) 2740.
[24] I.H. Campell, P.M. Fauchet, Solid State Commun. 58 (1986) 73.
[25] W.F. Zhang, Y.L. He, M.S. Zhang, Z. Yin, Q. Chen, J. Phys. D 33 (2000) 912.
[26] J.E. Spanier, R.D. Robinson, F. Zhang, S. Chan, I.P. Herman, Phys. Rev. B 64 (2001) 245407.
[27] T. Takagahara, K. Takeda, Phys. Rev. B 46 (1992) 15578.
[28] C. Zhi, Y. Bando, C. Tang, D. Golberg, J. Phys. Chem. B 110 (2006) 8548.
[29] F. Gu, S.F. Wang, M.K. Lii, G.J. Zhou, D. Xu, D.R. Yuan, J. Phys. Chem. B 108 (2004) 8119.